Microscopic description of superallowed α-decay transitions

Monika Patial,* R. J. Liotta, and R. Wyss
Royal Institute of Technology (KTH), Alba Nova University Center, SE-10691 Stockholm, Sweden
(Received 4 March 2016; published 26 May 2016)

It was recently found that the formation probabilities of α particles in Te isotopes are larger than the corresponding probabilities in Po isotopes. We have done a full microscopic calculation within the framework of the multistep shell model to analyze in detail the formation probabilities and subsequent decays of α particles from ^{212}Po and ^{104}Te. We have also calculated the spectra of these two decaying nuclei and found that the tentatively assigned spin (18^+) at 2.922 MeV in ^{212}Po (National Nuclear Data Center, www.nndc.bnl.gov) is predicted to be a state 16^+. We also present for the first time the full energy spectrum of ^{104}Te. The evaluated formation amplitudes in both nuclei show that in ^{104}Te there is indeed a superallowed α-decay transition.

DOI: 10.1103/PhysRevC.93.054326

I. INTRODUCTION

In recent years, great efforts have been made to study the neutron-deficient Te isotopes near the $N = Z = 50$ closed shells. One of the probes used in this search was the very elusive radioactive decay by emission of α particles [1]. Soon afterwards the striking feature that the α-decay process measured in light Te isotopes carries a preformation factor that is larger than the one in the classic decays of Po isotopes was found. The α-decay transitions from light Te isotopes were therefore called "superallowed" [2]. This was perhaps expected because around the ^{100}Sn core the valence nucleons, both neutrons and protons, move in the same single-particle (sp) shells, thus enhancing the neutron-proton interaction [3]. However only recently it has been experimentally possible to explore the α-decay channels in this very unstable region of the nuclear chart. Even other properties beyond α decay itself were possible to be investigated through α-decay probes. In particular, through the $^{109}\text{Xe} \rightarrow {}^{105}\text{Te} \rightarrow {}^{101}\text{Sn}$ α-decay chain the low-lying sp states in ^{101}Sn were observed [4].

The superallowed character of the α-decay transitions from light Te isotopes was established by examining reduced decay widths [2]. To analyze these transitions one has to formulate a theory that will describe in a reliable fashion the emission of the α particle. The decay itself proceeds in two steps. In the first step the four nucleons in the parent nucleus that eventually constitute the α particle get clustered together. In the second step the α particle thus formed on the surface of the daughter nucleus penetrates the Coulomb and centrifugal barriers. While the evaluation of the penetration probability is a relatively easy task, the assessment of the formation probability is a very difficult undertaking. Gamow explained the decay including only the penetration of an already formed α particle. To obtain the proper units, Gamow also introduced the concept of "assault frequency," which is an effective quantity without any quantum mechanics validity. This theory has been extremely successful in explaining relative decay widths, but cannot describe absolute decays. Yet because the calculation of the penetrability is very easy, the theory has been applied in many situations, trying to get the absolute decay widths by adjusting effective parameters, such as the assault frequency, to fit the corresponding decay width. These effective theories are very useful because they are easy to apply and therefore they help experimentalists to estimate the probability that the nucleus would decay through the channel under consideration. However this procedure does not evaluate the formation amplitude but rather takes it as a free parameter, albeit with other names. It is therefore not suitable for our purposes.

Another method which is rather successful is the cluster model. In this model the α particle is assumed to be already formed. By using a proper mean field acting between the α particle and the daughter nucleus and by a reasonable determination of the number of nodes of the corresponding wave function, one can describe well spectra of spherical nuclei [5,6] as well as deformed nuclei [7]. However in this model the interactions among the nucleons forming the α particle, in particular, the neutron-proton interaction, do not enter and therefore this model is not suitable for our purpose.

Finally, there is the microscopic calculation of the formation amplitude, which in principle does not include any free parameter, as described, e.g., in Ref. [8].

We briefly present this microscopic theory in Sec. II. In Sec. III we present the results of our calculations and in Sec. IV we present a summary and our conclusions.

II. FORMALISM

The proper expression for the decay width, taking into account all elements entering in the decay process, was first given by Thomas [9] as

$$\Gamma_L(R) = 2\gamma_L^2(R) P_L(R), \tag{1}$$

where R is the distance from the center of the daughter nucleus to the α particle and L is the angular momentum carried by the outgoing α particle. The reduced-width amplitude $\gamma_L(R)$ is given by

$$\gamma_L(R) = \left(\frac{\hbar^2 R}{2\mu}\right)^{1/2} F_L(R), \tag{2}$$

*Corresponding author: patial@kth.se

where $F_L(R)$ is the α-particle formation amplitude at the point R and μ is the α-particle reduced mass. The formation amplitude is given by

$$F_L(R) = \int d\xi_\alpha d\xi_D d\hat{R}[\phi_\alpha(\xi_\alpha)\psi_D(\xi_D)Y_L(\hat{R})]^*_{\alpha_4,\nu_4}\psi_P(\xi_\alpha\xi_D;R), \tag{3}$$

where ϕ and ψ are internal wave functions and ξ's are internal coordinates. For details see Refs. [8,9]. The penetrability is written as

$$P_L(R) = \frac{kR}{G_L^2(R)+F_L^2(R)}, \tag{4}$$

where F and G are the regular and irregular Coulomb functions, respectively, and $k = \mu v/\hbar$, v being the velocity of the outgoing α particle.

A. The multistep shell model

In the multistep shell model (MSM) one solves the shell-model equations in several steps [10]. One first chooses a single-particle representation. In the second step one adopts a two-particle interaction to evaluate the two-particle states. The three-particle system is solved in terms of two-particle states times one-particle states. The four-particle states can be solved in terms of (a) two-particle states times themselves (as is done here) or (b) one-particle states times the three-particle states previously evaluated, or in terms of a linear combination of (a) and (b). For more particles one proceeds in a similar fashion, building the MSM representation in terms of correlated states. One drawback of the MSM basis is that it may violate the Pauli principle as well as counting states more than once. To correct these deficiencies one must evaluate the overlap matrix among the basis states to build a complete basis. However, in the cases to be studied in this article, which are two-proton ($2p$) times two-neutron ($2n$) systems, the $2p2n$ MSM basis is complete, because the Pauli principle does not act between protons and neutrons.

We thus study systems with two protons and two neutrons outside a double-magic core. The corresponding MSM wave function for state α_4 is

$$\mid \alpha_4\rangle = \sum_{\alpha_2,\beta_2} X(\alpha_2\beta_2;\alpha_4)[P^+(\alpha_2)P^+(\beta_2)]_{\alpha_4} \mid 0\rangle, \tag{5}$$

where α_2 (β_2) labels two-proton (two-neutron) states, i.e.,

$$\mid \alpha_2\rangle = P^\dagger(\alpha_2)\mid 0\rangle, \quad \text{with } P^\dagger(\alpha_2) = \sum_{i<j} X(ij;\alpha_2)c_i^\dagger c_j^\dagger,$$
$$\mid \beta_2\rangle = P^\dagger(\beta_2)\mid 0\rangle, \quad \text{with } P^\dagger(\beta_2) = \sum_{p<q} X(pq;\beta_2)a_p^\dagger a_q^\dagger. \tag{6}$$

The index i (p) labels proton (neutron) sp states, $c_i^\dagger$ ($a_p^\dagger$) are sp creation operators and $X(ij;\alpha_2)$ [$X(pq;\beta_2)$] are the corresponding wave function amplitudes. The proton-proton (neutron-neutron) interaction provides the two-particle energies and wave functions, that is, the creation operators $P^\dagger(\alpha_2)$ and $P^\dagger(\beta_2)$. In this $2p2n$ case the MSM dynamical equation is

$$\sum_{\alpha_2'\beta_2'}\big[(W_{\alpha_2}+W_{\beta_2})\delta_{\alpha_2,\alpha_2'}\delta_{\beta_2,\beta_2'} + \langle\alpha_2\beta_2;\alpha_4 \mid V_{pn}\mid\alpha_2'\beta_2';\alpha_4\rangle\big]X(\alpha_2'\beta_2';\alpha_4) = W_{\alpha_4}X(\alpha_2\beta_2;\alpha_4), \tag{7}$$

where W_{α_2} (W_{β_2}) is the two-proton (two-neutron) correlated energy and V_{pn} is the proton-neutron (pn) interaction. The eigenvalue W_{α_4} is the $2p2n$ energy and the eigenvectors $X(\alpha_2\beta_2;\alpha_4)$ are the amplitudes which provide the wave function (5). One can see from Eq. (7) that if one neglects the pn interaction (as has been done in, e.g., Refs. [11,12]) only one configuration contributes to Eq. (5). In other words, the values of the amplitudes $X(\alpha_2\beta_2;\alpha_4)$ are determined by the pn interaction. The pn interaction matrix element has the form

$$\begin{aligned}\langle\alpha_2\beta_2;\alpha_4 \mid V_{pn} \mid \alpha_2'\beta_2';\alpha_4\rangle &= (-1)^{\beta_2+\beta_2'+\alpha_4}\\ &\times[\alpha_2]^{1/2}[\alpha_2']^{1/2}[\beta_2]^{1/2}[\beta_2']^{1/2}\sum_{ijk}\sum_{pqr}\sum_{\lambda}(-1)^{\lambda+q+i-j+k}[\lambda]\\ &\times\sum_l[l]\begin{Bmatrix}\alpha_2 & \alpha_2' & l\\ k & i & j\end{Bmatrix}\begin{Bmatrix}p & i & \lambda\\ k & r & l\end{Bmatrix}\\ &\times\begin{Bmatrix}\beta_2 & \beta_2' & l\\ r & p & q\end{Bmatrix}\begin{Bmatrix}\beta_2 & \beta_2' & l\\ \alpha_2' & \alpha_2 & \alpha_4\end{Bmatrix}\\ &\times Y(ij;\alpha_2)Y(pq;\beta_2)Y(kj;\alpha_2')Y(rq;\beta_2')\langle ip;\lambda\mid V_{pn}\mid kr;\lambda\rangle,\end{aligned} \tag{8}$$

where $Y(ij;\alpha_2) = \sqrt{1+\delta_{ij}}X(ij;\alpha_2)$. Notice that Latin and Greek letters label the states as well as the corresponding angular momenta, as seen in the 6-j symbols above. The rest of the notation is standard. Thus $[\alpha_2] = 2\alpha_2+1$.

In r representation the $2p2n$ wave function (5) can be written as

$$\begin{aligned}\psi_P(\xi_\alpha\xi_D;\vec{R}) &= \psi_P(\vec{r}_1,\vec{r}_2,\vec{r}_3,\vec{r}_4;\xi_D)\\ &= \sum_{\alpha_2,\beta_2}X(\alpha_2\beta_2;\alpha_4)\big[\psi_{\alpha_2}(\vec{r}_1,\vec{r}_2)\psi_{\beta_2}(\vec{r}_3,\vec{r}_4)\big]_{\alpha_4,\nu_4}\psi_D(\xi_D),\end{aligned} \tag{9}$$

where the label P (D) indicates the parent (daughter) nucleus. The internal coordinates ξ_α and ξ_D correspond to the α particle and the daughter nucleus, respectively, and r_i is the coordinate of the nucleon i.

There are two regions in the decay process. In the internal region, that is, in the parent nucleus, the two protons and two neutrons that eventually constitute the α particle move in the field generated by the other nucleons. In our two cases this field is generated by the double-magic cores ^{100}Sn(gs) and ^{208}Pb(gs). One can therefore describe the motion of the nucleons in terms of the shell model by using an harmonic oscillator representation. In the external region we describe the motion of the already formed α particle around the core as a two-body system interacting through the Coulomb and centrifugal potentials. We use in this region outgoing boundary

conditions, which are described in Sec. III. The important feature to be stressed here is that the decaying α particle is formed on the surface of the daughter nucleus. When investigating the correlations that induce the creation of the α particle, we analyze the formation amplitude $F_{\alpha_4}(R)$ in the region R around the nuclear surface.

To evaluate the formation amplitude we replace the wave function (9) in Eq. (3) and make a transformation to relative coordinates (for details see, e.g., Ref. [13]). One gets

$$F_{\alpha_4}(R) = \sum_{\alpha_2\beta_2} X(\alpha_2\beta_2;\alpha_4) \sum_{N_\pi} T(\alpha_2 N_\pi) \sum_{N_\nu} T(\beta_2 N_\nu) \times \sum_{N_\alpha} \langle N_\pi \alpha_2 N_\nu \beta_2; \alpha_4 \mid 00 N_\alpha \alpha_4; \alpha_4 \rangle \mathcal{R}_{N_\alpha \alpha_4}(R) = \sum_{N_\alpha} \mathcal{F}_{N_\alpha \alpha_4} \mathcal{R}_{N_\alpha \alpha_4}(R), \quad (10)$$

where $\mathcal{F}_{N_\alpha\alpha_4}$ is a straightforward coefficient, $\langle N_\pi\alpha_2 N_\nu\beta_2;\alpha_4 \mid 00N_\alpha\alpha_4;\alpha_4\rangle$ is a Moshinsky bracket, and $\mathcal{R}_{N_\alpha\alpha_4}(R)$ is the radial wave function corresponding to the outgoing α particle. As mentioned above, we adopt for this an outgoing (Gamow) function.

In the derivation of Eq. (10) one considers that the intrinsic α-particle wave function is the product of the lowest-harmonic oscillator wave functions. That means that the quantum numbers of the α particle, i.e., the principal quantum number n and the orbital angular momentum l, are $n_p = l_p = n_n = l_n = 0$. Moreover, all are singlet states, i.e., $S_p = S_n = 0$.

The functions T are given by

$$T(\alpha_2 N_\pi) = \sum_i Y(ii,\alpha_2)(-1)^{l_i+1/2+j_i+\alpha_2} \frac{(2j_i+1)}{\sqrt{2}} \times \begin{Bmatrix} j_i & l_i & 1/2 \\ l_i & j_i & \alpha_2 \end{Bmatrix} \langle 00 N_\pi \alpha_2; \alpha_2 \mid n_i l_i n_i l_i \alpha_2 \rangle + \frac{1}{2} \sum_{i<j} Y(ij;\alpha_2) \sqrt{(2j_i+1)(2j_j+1)} \times \begin{Bmatrix} j_i & l_i & 1/2 \\ l_j & j_j & \alpha_2 \end{Bmatrix} \Big[(-1)^{l_i+1/2+j_j+\alpha_2} \times \langle 00 N_\pi \alpha_2; \alpha_2 \mid n_i l_i n_j l_j \alpha_2 \rangle + (-1)^{l_j+1/2+j_i+\alpha_2} \langle 00 N_\pi \alpha_2; \alpha_2 \mid n_j l_j n_i l_i \alpha_2 \rangle \Big] \quad (11)$$

and a similar expression for $T(\beta_2 N_\nu)$.

With the formation amplitude thus evaluated the reduced width (2) and the width (1) can be calculated.

III. APPLICATIONS

We analyze the α-particle emission from ^{212}Po and ^{104}Te using the formalism presented above.

A. ^{212}Po

The first two steps in our MSM treatment is to choose the single- and two-particle states. An excellent choice for these quantities has been provided long ago by Kuo and Harling (KH) in Ref. [14] (the so-called Approximation 2, which includes particle-hole excitations in the two-particle matrix elements).

In the KH calculation the proton sp states correspond to the $N = 5$ major shell, i.e., $0h_{9/2}$, $1f_{7/2}$, $0i_{13/2}$, $1f_{5/2}$, $2p_{3/2}$, and $2p_{1/2}$, while the neutron sp states correspond to the $N = 6$ shell, i.e., $1g_{9/2}$, $0i_{11/2}$, $0j_{15/2}$, $2d_{5/2}$, $3s_{1/2}$, $1g_{7/2}$, and $2d_{3/2}$. All the two-particle states provided by this set of sp states are included in our MSM calculation. The pn matrix elements between sp states appearing in Eq. (8) were extracted from the ^{210}Bi KH energies and wave functions.

To assess the quality of the procedure used here we show in Fig. 1 the calculated ^{212}Po spectrum. The calculated ^{212}Po ground-state (gs) energy is -19.09 MeV, to be compared with the experimental value, which is -19.34 MeV. The calculated yrast-state energies agree with the corresponding experimental values within an energy range of 80 keV. An exception is the (tentative) experimental state (18^+_1), with an energy that differs from the corresponding theoretical value by 295 keV. However the calculated energy of state 16^+_1 is 2.988 MeV, which is very close to the experimental state (18^+_1) with an energy measured at 2.922 MeV. We therefore conclude that the measured state (18^+_1) is in reality 16^+_1.

The good agreement between theory and experiment seen above indicates that the calculations presented here are reliable.

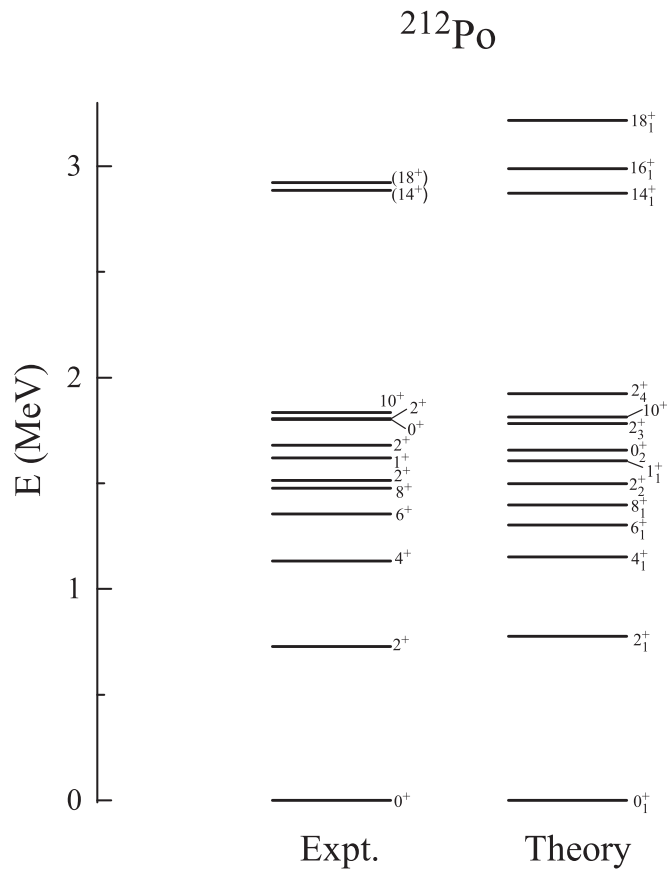

FIG. 1. Experimental spectrum [15] of ^{212}Po and the corresponding theoretical one.

TABLE I. Amplitudes $X(\alpha_2\beta_2;\alpha_4) = X[^{210}\mathrm{Po}(\alpha_2) \otimes ^{210}\mathrm{Pb}(\beta_2); \alpha_4]$ for α_2 and β_2 yrast states, corresponding to ^{212}Po(gs).

^{210}Po(α_2)	^{210}Pb(β_2)	$X(\alpha_2\beta_2;\alpha_4)$
0_1^+	0_1^+	0.913
2_1^+	2_1^+	−0.253
4_1^+	4_1^+	0.122
6_1^+	6_1^+	0.064
8_1^+	8_1^+	0.030

A measure of the importance of the *pn* interaction in this nuclear region can be gathered by the mixing of configurations in the wave function of the state ^{212}Po(gs). One expects that this state is mainly defined by the monopole isovector pairing force; i.e., that it can be written as $|^{212}\mathrm{Po(gs)}\rangle = |^{210}\mathrm{Pb(gs)} \otimes ^{210}\mathrm{Po(gs)}\rangle$. This would be the case if the *pn* interaction were negligible [11,12]. A measure of the plausibility of this assumption is to compare the energy E_0 of that state, i.e., $E_0 = E(^{210}\mathrm{Pb(gs)}) + E(^{210}\mathrm{Po(gs)}) = -17.91$ MeV, with the experimental energy of the state $^{212}\mathrm{Po(gs)} = -19.34$ MeV. That is, the *pn* correlation energy is −1.43 MeV. This may seem a large correlation. However, one sees in Table I that the configuration above is indeed dominant, indicating that the *pn* interaction does not play a big role in this case. This feature is expected because neutrons and protons move in different parity shells and their overlaps, i.e., the corresponding *pn* matrix elements, are small. This conclusion is strengthen by comparing the *pn* correlated energy above with the much larger one in the Sn region, where neutrons and protons occupy the same shells.

With the wave function amplitudes thus evaluated, we calculate the formation amplitudes corresponding to the ground state of ^{212}Po using Eq. (10). As explained above, for the α-particle wave function $\mathcal{R}_{N_\alpha\alpha_4}(R)$ in Eq. (10), we use outgoing boundary conditions. We evaluate it by using the computer code GAMOW [16]. As the central field we adopt a Woods-Saxon (WS) potential with parameters ($r_0 = 1.315$ fm, $a = 0.65$ fm) of Ref. [17]. The depth of the potential is adjusted to match the Q_α value of the outgoing α particle.

It is important to point out that in Eq. (10) the coefficient $\mathcal{F}_{N_\alpha\alpha_4}$ is strongly dependent upon the number of nodes N_α. In our case of the α formation from the ground state it is $\alpha_4 = 0$ and $\mathcal{F}_{N_\alpha=11} = 1.7 \times 10^{-2}$, $\mathcal{F}_{N_\alpha=12} = -8.0 \times 10^{-4}$, and $\mathcal{F}_{N_\alpha=13} = 1.4 \times 10^{-5}$. Therefore in practice only the largest value of $\mathcal{F}_{N_\alpha\alpha_4}$ has to be taken into account. This corresponds to the minimum principal quantum number, i.e., $N_\alpha = N_\alpha^{\min} = 11$. We found the remarkable property that in the outgoing wave function $\mathcal{R}_{N_\alpha\alpha_4}(R)$, obtained as explained above, the number of nodes coincides with $N_\alpha^{\min}$, as is indeed necessary.

With the formation amplitude thus obtained we evaluated the decay width (1). In Fig. 2, we present the corresponding calculated half-life as a function of the distance R between the daughter nucleus and the α particle. One sees that the half-life is independent of R at distances outside the daughter nucleus, as it should be. This is a result of the short range of the nuclear interaction, which makes it so that the wave function of the α particle at distances outside the range of the nuclear interaction is exactly the same as the Coulomb function that generates the penetrability. The penetrability increases exponentially and the formation probability decreases exponentially at large distances. The product of these two functions is constant outside the daughter nucleus. But at very large distances all functions are strongly exponential and the precision errors may induce variations that are not physically meaningful. The constancy of the calculated half-life seen in Fig. 2 enforces the argument that the calculation is reliable.

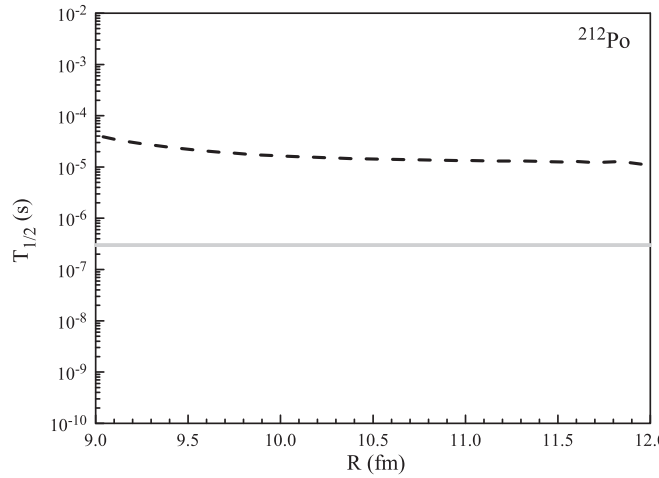

FIG. 2. Calculated half-life of ^{212}Po as a function of the distance between the α particle and the daughter nucleus. The solid line indicates the corresponding experimental value [15].

The calculated half-life of ^{212}Po shows a small variation in the significant range of radial distances in Fig. 2. We therefore assign the average value of 15 μs for this half-life.

Yet, the half-life thus calculated is 2 orders of magnitude larger than the corresponding experimental value. In effective theories, where the preformation probability is a parameter extracted from fittings to previous experimental values, theory and experiment agree reasonably well, as seen in Refs. [18,19]. However, in microscopic theories the large divergence between calculated and experimental half-lives is not an unexpected feature. It has been pointed out in Refs. [11,12] that one should include high-lying configurations to get better agreement with experiment. It has been found in Ref. [20] that these high-lying configurations are necessary to explain the clustering among the two neutrons and the two protons that form the α particle, but it has to be pointed out that already within the sp states included here there is a sizable clustering.

Recently it was found that in processes where the α particle plays a role, like in α decay, one needs a cluster component in the shell-model wave function [21]. This was already found in Ref. [22]. Within our shell-model space, we evaluated the α-formation amplitude (10) shown in Fig. 3. One sees that this formation amplitude coincides with the equivalent one in Ref. [22]. However the formation amplitude including cluster components is nearly exactly 1 order of magnitude larger than the pure shell-model one [cf. Figs. 4(a) and 4(c) in that reference]. With the formation amplitude thus increased by

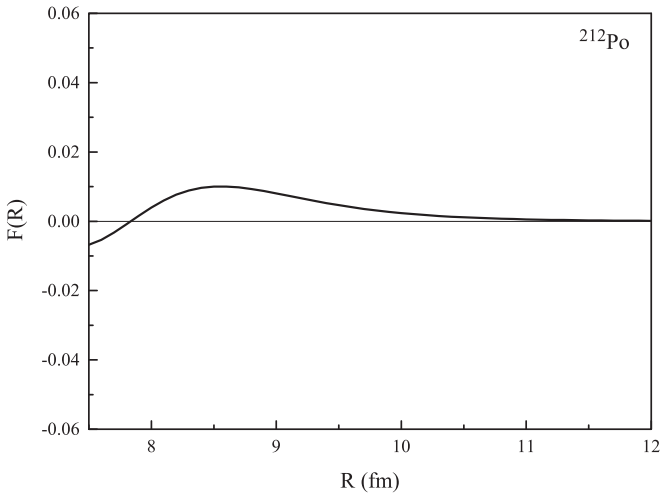

FIG. 3. The α formation amplitude (in fm$^{-1/2}$) for ^{212}Po as a function of the radial distance.

the factor of 10 found in Ref. [22] our calculated half-life coincides with the experimental one.

B. ^{104}Te

There has been a strong interest in nuclei around ^{100}Sn, which is the heaviest self-conjugate nucleus that has been detected so far. This interest is partly due to the expected increased proton-neutron correlations in these nuclei. This may induce a variety of enhanced phenomena, like manifestations of isoscalar pairing modes and increased α-decay transitions.

To calculate the spectrum of the nucleus ^{104}Te, with two protons and two neutrons outside the ^{100}Sn core, we proceed as we did above with the equivalent nucleus ^{212}Po. We adopt a set of single-particle states corresponding to the shell $N = 4$ that describes well light Sn isotopes [23]. These sp states are the same for neutrons and protons. The energies, in MeV, are $\epsilon_{1d_{5/2}} = -10.9$, $\epsilon_{0g_{7/2}} = -10.7$, $\epsilon_{2s_{1/2}} = -9.5$, $\epsilon_{1d_{3/2}} = -8.9$, and $\epsilon_{0h_{11/2}} = -8.5$. The binding energy of state $1d_{5/2}$ at -10.95 MeV was taken from the measured value in ^{101}Sn [15]. We chose a realistic and reliable interaction that, as in the case of KH, includes virtual particle-hole excitations in the matrix elements, thus describing well nuclei in this region [24]. As an example, we show in Fig. 4 the calculated spectra of the two-proton (^{102}Te) and two-neutron (^{102}Sn) nuclei. The scarce experimental data that are available are very well explained by the calculation. With the two-particle states thus obtained, the calculation of the spectrum of ^{104}Te was performed in the same way as in the previous section. The *pn* interaction matrix elements among sp states was also obtained from Ref. [24]. Including all possible two-particle states we calculated the energy spectrum shown in Fig. 5. It is worthwhile to point out that this spectrum is presented here for the first time. This could be helpful to experimentalists planning measurements in this region of the nuclear chart, which are expected to be performed in the near future.

Note that the *pn* interaction lowers the energy of the ground state of ^{104}Te by 5.7 MeV with respect to the energy of the

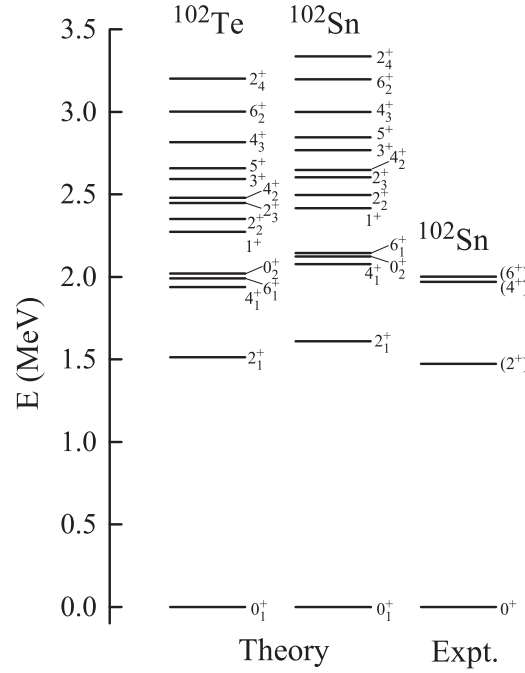

FIG. 4. Calculated spectra of ^{102}Te and ^{102}Sn and the corresponding available experimental data in ^{102}Sn [15]. For clarity, only positive-parity states are shown, though in the calculations both positive- and negative-parity states are taken into account.

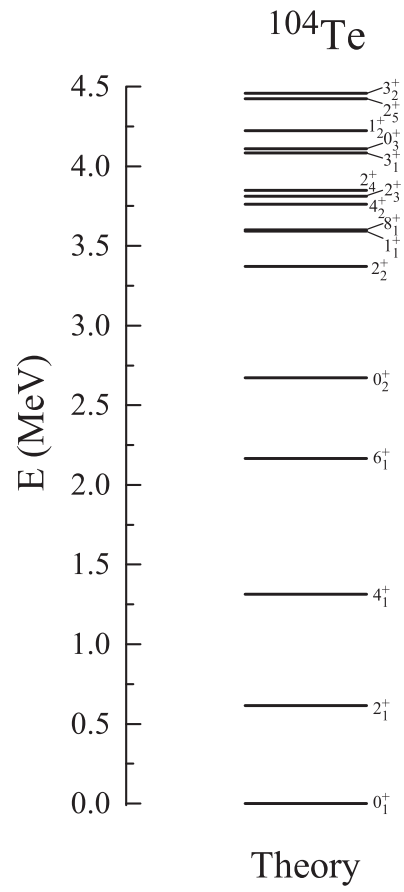

FIG. 5. Calculated energy level scheme for ^{104}Te.

TABLE II. Amplitudes $X(\alpha_2\beta_2;\alpha_4) = X[^{102}\text{Te}(\alpha_2)\otimes^{102}\text{Sn}(\beta_2);\alpha_4]$ for α_2 and β_2 yrast states, corresponding to ^{104}Te(gs).

^{102}Te(α_2)	^{102}Sn(β_2)	$X(\alpha_2\beta_2;\alpha_4)$
0_1^+	0_1^+	0.544
2_1^+	2_1^+	0.483
4_1^+	4_1^+	0.318
6_1^+	6_1^+	0.228

uncorrelated state $|^{104}\text{Te(gs)}\rangle = |^{102}\text{Te(gs)}\otimes^{102}\text{Sn(gs)}\rangle$. This can be compared with the value of 1.43 MeV in ^{212}Po discussed in the previous section, but the importance of the *pn* interaction in this nuclear region can also be seen by analyzing the wave function of the state $|^{104}\text{Te(gs)}\rangle$. This we show in Table II, where the amplitudes corresponding to the configurations $|^{102}\text{Te}(\alpha_2)\otimes^{102}\text{Sn}(\beta_2)\rangle$ are given. One sees that the pairing monopole mode is not as dominant as it was in the Pb region.

We evaluated the α-formation amplitude in the state ^{104}Te(gs) shown in Fig. 6, using the same Woods-Saxon potential and the same procedure as for ^{212}Po. In particular, here, as was the case for ^{212}Po, only the minimum number of nodes N_α in Eq. (10) is relevant. One sees from Fig. 6 that the α-particle formation correlations present in Te but not in Po isotopes (c.f. Fig. 3), explains the superallowed character of the α transitions in Te.

To evaluate the half-life one has to know the experimental Q_α value in ^{104}Te, which is not available. To obtain this we have done a linear fitting to the binding energies of neighboring nuclei as shown in Fig. 7. We thus get the total binding energy for ^{104}Te as 848.534 MeV. Note that the total binding energy estimated in this simple way is in close agreement with the semiempirical value given by Myers and Swiatecki [25]. Moreover, the corresponding Q_α value is obtained as 5.059 MeV, which is also in good agreement with the extrapolated α-decay energy of 5.053 MeV in Ref. [26]. The calculated half-life as a function of the distance R is

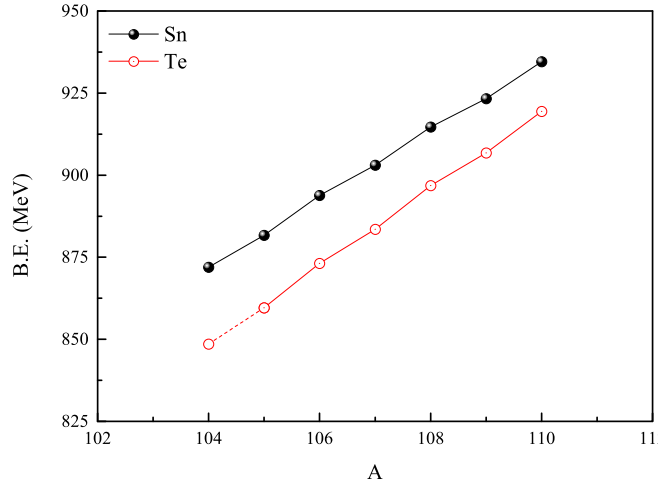

FIG. 7. Total binding energy as a function of A.

presented in Fig. 8. Again in this case it is seen that the half-life is independent of R at large distances, giving reliability to the calculation. We assign the theoretical half-life of ^{104}Te as 1.5 μs. However, one expects that the corresponding experimental value should be 2 orders of magnitude smaller than the theoretical one, as discussed above for the case of ^{212}Po(gs).

IV. SUMMARY AND CONCLUSIONS

We have studied the structure and the α-formation probability corresponding to the nuclei ^{212}Po and ^{104}Te using a full microscopic formalism, namely, the multistep shell-model method. We found that the tentatively assigned (18^+) at 2.922 MeV in ^{212}Po [15] is instead a 16^+ state. We have also presented the level scheme of the nucleus ^{104}Te, which could be of importance for future experimental searches in light Te isotopes.

We evaluated the formation probabilities and the α-decay widths in ^{104}Te(gs) and ^{212}Po(gs). We found that the proton-neutron correlations are much more important in Te than in Po. This is expected, because the active neutrons and protons

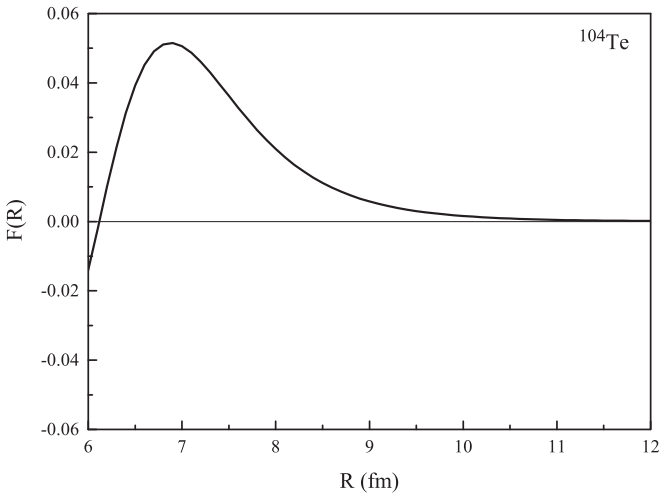

FIG. 6. The α formation amplitude (in fm$^{-1/2}$) for ^{104}Te as a function of the radial distance.

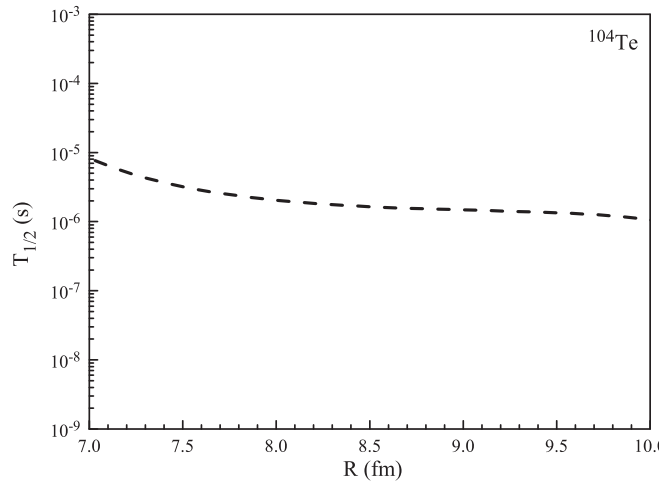

FIG. 8. Calculated half-life of ^{104}Te. Notice that no experimental data are available in this case.

move in the same orbits in Te, but in different ones in Po. As a result ^{212}Po(gs) becomes a near pure monopole isovector state, while ^{104}Te(gs) presents strong mixing with other (multipole) states. Another consequence of the proton-neutron correlations is that the α-particle formation probability in ^{104}Te is 4.85 times larger than that in ^{212}Po, thus attesting that in the Te region there is a superallowed α-decay transition.

ACKNOWLEDGMENTS

We express our gratitude to Morten Hjorth-Jensen for providing us with the two-body interaction matrix elements. This work was supported by the Royal Institute of Technology, Stockholm, and the Swedish Research Council (VR) under Grants No. 621-2012-3805 and No. 621-2013-4323.

[1] Z. Janas, C. Mazzocchi, L. Batist, A. Blazhev, M. Górska, M. Kavatsyuk, O. Kavatsyuk, R. Kirchner, A. Korgul, M. La Commara *et al.*, Eur. Phys. J. A **23**, 197 (2005).
[2] S. N. Liddick, R. Grzywacz, C. Mazzocchi, R. D. Page, K. P. Rykaczewski, J. C. Batchelder, C. R. Bingham, I. G. Darby, G. Drafta, C. Goodin *et al.*, Phys. Rev. Lett. **97**, 082501 (2006).
[3] R. D. Macfarlane and A. Siivola, Phys. Rev. Lett. **14**, 114 (1965).
[4] I. G. Darby, R. K. Grzywacz, J. C. Batchelder, C. R. Bingham, L. Cartegni, C. J. Gross, M. Hjorth-Jensen, D. T. Joss, S. N. Liddick, W. Nazarewicz *et al.*, Phys. Rev. Lett. **105**, 162502 (2010).
[5] B. Buck, A. C. Merchant, and S. M. Perez, Phys. Rev. C **45**, 2247 (1992).
[6] F. Hoyler, P. Mohr, and G. Staudt, Phys. Rev. C **50**, 2631 (1994).
[7] B. Buck, A. C. Merchant, and S. M. Perez, Phys. Rev. C **85**, 054302 (2012).
[8] R. G. Lovas, R. J. Liotta, A. Insolia, K. Varga, and D. S. Delion, Phys. Rep. **294**, 265 (1998).
[9] R. G. Thomas, Prog. Theor. Phys. **12**, 253 (1954).
[10] R. J. Liotta and C. Pomar, Nucl. Phys. A **382**, 1 (1982).
[11] I. Tonozuka and A. Arima, Nucl. Phys. A **323**, 45 (1979).
[12] F. A. Janouch and R. J. Liotta, Phys. Lett. B **82**, 329 (1979).
[13] D. S. Delion, *Theory of Particle and Cluster Emission*, Lecture Notes in Physics (Springer, Berlin, 2010).
[14] T. T. S. Kuo, G. H. Harling, and STATE UNIV OF NEW YORK STONY BROOK, *Two-Particle and Two-Hole States in the Pb Region* (Defense Technical Information Center, Washington, DC, 1971).
[15] http://www.nndc.bnl.gov.
[16] T. Vertse, K. F. Pal, and Z. Balogh, Comput. Phys. Commun. **27**, 309 (1982).
[17] R. M. DeVries, J. S. Lilley, and M. A. Franey, Phys. Rev. Lett. **37**, 481 (1976).
[18] C. Xu, Z. Ren, G. Röpke, P. Schuck, Y. Funaki, H. Horiuchi, A. Tohsaki, T. Yamada, and B. Zhou, Phys. Rev. C **93**, 011306 (2016).
[19] Y. Ren and Z. Ren, Phys. Rev. C **85**, 044608 (2012).
[20] F. A. Janouch and R. J. Liotta, Phys. Rev. C **27**, 896 (1983).
[21] D. S. Delion and R. J. Liotta, Phys. Rev. C **87**, 041302 (2013).
[22] K. Varga, R. G. Lovas, and R. J. Liotta, Nucl. Phys. A **550**, 421 (1992).
[23] N. Sandulescu, J. Blomqvist, and R. J. Liotta, Nucl. Phys. A **582**, 257 (1995).
[24] M. Hjorth-Jensen, T. T. S. Kuo, and E. Osnes, Phys. Rep. **261**, 125 (1995).
[25] W. D. Myers and W. J. Swiatecki, Nucl. Phys. **81**, 1 (1966).
[26] C. Xu and Z. Ren, Phys. Rev. C **74**, 037302 (2006).